Hindawi
Shock and Vibration
Volume 2021, Article ID 6647162, 13 pages
https://doi.org/10.1155/2021/6647162

Research Article

A Novel Circular Plate Acoustic Energy Harvester for Urban Railway Noise

Tian-Chen Yuan,[1] Fei Chen,[1] Jian Yang ,[1] Rui-Gang Song,[1] and Yong Kong[2]

[1]*School of Urban Railway Transportation, Shanghai University of Engineering Science, Shanghai 201620, China*
[2]*School of Electronic and Electrical Engineering, Shanghai University of Engineering Science, Shanghai 201620, China*

Correspondence should be addressed to Jian Yang; yang2580@sues.edu.cn

Received 10 December 2020; Revised 27 July 2021; Accepted 9 September 2021; Published 20 September 2021

Academic Editor: M.I. Herreros

To harvest acoustic energy from urban railways, a novel and practical acoustic energy harvester is developed. The harvester consists of a piezoelectric circular plate and a Helmholtz resonator. Based on the field test data of urban railways, the resonance frequencies of the piezoelectric circular plate and the Helmholtz resonator are near 800 Hz. The Helmholtz resonator is designed to amplify the sound pressure. Thus, a lumped parameter model is established. The piezoelectric circular plate is used to convert mechanical energy into electrical energy. The simulation results show that the output power of the harvester is approximately 25 μW and the maximum voltage is 0.149 V under the excitation of urban railway noise. The experiment device is also developed. The maximum output power of the harvester is 8.452 μW, and the maximum voltage is 0.082 V. The experimental and the numerical results are in good agreement and demonstrate the effectiveness of the proposed acoustic energy harvester.

1. Introduction

Harvesting energy from the environment can generate power to drive low-power electronic devices, such as wireless sensors and health-monitoring sensors [1, 2]. Many scientists have investigated methods to harvest energy from vibration energy [3], acoustic energy [4, 5], wind energy [6], solar energy [7], and ocean waves [8]. A substantial amount of literature has focused on harvesting the linear or nonlinear vibration energy or the radiated noise caused by the structure vibration [4, 5, 9–15]. Therefore, energy harvesting is a promising research field with huge potential.

At present, the high-speed transit of urban railway vehicles has caused serious noise pollution. Double-sided microcellular foam noise barriers have been developed [16] and installed in the retaining wall of station platforms. Urban railway noise can be reduced through sound absorption and prevention of sound propagation. Thus, a noise energy harvester must be developed to harvest wheel-rail noise and to drive some track monitoring equipment.

On the basis of the piezoelectric effect, Li et al. developed an acoustic energy harvesting mechanism to harvest traveling sound at low audible frequency. The harvester contains a quarter-wavelength straight tube resonator with piezoelectric cantilever plates placed inside the tube [17]. Gao et al. developed acoustic energy harvesting for low-frequency sound in a subwavelength system. This harvester contains eight multiple-cavity units. Moreover, it has rich compound Mie resonances and strong robustness [18]. In another study, Yuan et al. proposed a multifunctional acoustic metastructure to realize both effective low-frequency sound isolation and acoustic energy harvesting. The system exhibits excellent noise isolation in the low-frequency band, and the incident sound energy can be converted into electrical energy by the piezoelectric patch [19].

All the above mentioned studies focus on acoustic energy harvesting by tube structure. However, the Helmholtz resonator is an effective method to amplify the sound pressure. Thus, many researchers have developed acoustic energy harvesters with Helmholtz resonators. For example, an electromechanical Helmholtz resonator with a

polyvinylidene fluoride (PVDF) piezoelectric composite cantilever for harvesting acoustic energy was proposed [20]. The results show a maximum power of 0.19 μW with sound waves of 15 Pa (118 dB) at 850 Hz. Noh et al. investigated piezoelectric (PVDF composite) cantilevers with Helmholtz resonators to harvest acoustic energy. The generated power was approximately 0.1 μW through piezoelectric materials [21]. In addition, Yang et al. proposed an acoustic energy harvester consisting of a Helmholtz resonator and dual piezoelectric cantilever beams. Each beam consists of a magnet at the free end [22]. Yuan et al. designed an acoustic energy harvester that contains a Helmholtz resonator and a PVDF film to harvest acoustic energy from high-speed railways. The results of the experiment show that a single unit of the harvester can generate a maximum output voltage of 74.6 mV at 110 dB (SPL) [23]. An acoustic energy harvester with a piezoelectric generator and a Helmholtz resonator is also developed to harvest high-speed trains' noise in the passenger, cab, and between car sections [24]. Yuan et al. developed a helix structure for low-frequency acoustic energy harvesting. The acoustic resonance frequency is 175 Hz [25]. Atrah et al. developed and simulated an acoustic energy harvester with Helmholtz resonator. The resonance frequency is 3.5 kHz [26]. Khan also developed an acoustic energy harvester with a tapered Helmholtz resonator. A proof mass was attached to the piezoelectric plate [27].

To convert mechanical energy into electrical energy, the piezoelectric cantilever beam has been widely used [17, 20–23]. However, the circular piezoelectric plate is also an effective way to harvest energy. It has a high coupling coefficient [28], thus increasingly attracting researchers' attention in both acoustic energy harvesting and vibration energy harvesting [25–31]. Xue et al. [32] analyzed nonlinear characteristics of a circular piezoelectric plate near the resonance on the basis of von Karman theory. In the previous work, these authors also developed a circular piezoelectric plate array to harvest vibration energy from railways [33]. Although there are a lot of studies about developing a circular piezoelectric plate harvest with a Helmholtz resonator, the design is not specific to the engineering application. Most studies focus on the mid-high frequency range; for example, the frequency range of [27] is from 1100 Hz to 3450 Hz. However, mid-low-frequency sound sources are prevalent within the industrial environment [25], so it is important to investigate an acoustic energy harvester in the mid-low-frequency range.

In this study, a novel circular plate energy harvester with a Helmholtz resonator is developed to harvest acoustic energy from the urban railway systems. The noise characteristics are analyzed on the basis of the field test data of urban railways. The Helmholtz resonator and the circular piezoelectric plate are designed, modeled, and simulated. The resonance frequency is 831 Hz, which is lower than those in [26, 27]. The simulation results show that the proposed harvester can effectively generate electrical energy from the urban railway noise. The experiment system is also established, and the results of the experiment are in good agreement with the theoretical results. Therefore, the present work demonstrates the innovation and feasibility of the circular plate energy harvester with the Helmholtz resonator.

The manuscript is organized as follows. Section 2 describes the measurements and analyses of the urban railway noise. Section 3 presents the theoretical model of the acoustic energy harvester, and Section 4 presents the simulations of the acoustic energy harvester. Then, Section 5 shows the experiment results of the acoustic energy harvester and compares the analytical solutions with the results of the experiment. Lastly, Section 6 ends the paper with the concluding remark.

2. The Characteristics of Urban Railway Noise

The noises induced by urban railway vehicles can mainly be divided into wheel-rail noise, traction system noise, braking noise, aerodynamic noise, and track structure noise. When the vehicles are moving, the speed would generally be at 50 km/h to 80 km/h, and the wheel-rail noise is the main source of noise. The contribution of the wheel-rail noise for the total noise is far more than those of other kinds. In this study, the wheel-rail noise is the main object of noise energy harvesting.

To clarify the characteristics of the noise of rail transit, the authors measured the noise of rail transit on the spot. The measurements were taken from Songjiang University Town Station to Songjiang Xincheng Station of Shanghai Metro line 9. The distance between the two stations is approximately 800 m, and the speed of the vehicles through the measuring point is approximately 70 km/h. In the measurement process, a microphone was set in the internal shield wall. Then, the noise data were acquired. The measurement scheme diagram is shown in Figure 1.

The time domain of sound pressure is shown in Figure 2(a). The duration the train takes to pass through the station is approximately 7 s. The sampling frequency is 12 kHz. The train has six car formations, and the length of each train is 22.8 m. The sound pressure is mainly approximately 10 Pa, and its peak value can reach 25 Pa. The test vehicle has 24 wheel sets with 6 sections. Thus, 24 sound pressure peaks are represented in Figure 2(a).

The analysis of urban railway noise is the basis of energy harvesting. The frequency characteristics of urban railway noise determine the main design parameters of the noise energy harvester. The frequency domain of sound pressure is shown in Figure 2(b) by fast Fourier transform (FFT). The peak frequency of the sound pressure of urban railway noise is mainly concentrated in 500–1200 Hz.

Next, a 1/3 octave spectrum was obtained from the analysis of filtered noise data in the frequency domain, which is shown in Figure 3. The figure shows that the peak frequency band of the sound pressure is concentrated between 400 Hz and 1600 Hz. The noise energy is mainly concentrated in the 1/3 octave band of 500–1250 Hz. The 800 Hz frequency band has the largest contribution rate of noise energy, and it accounts for approximately 28% of the total energy. Therefore, the noise within the 800 Hz frequency band is the main object to harvest the energy of urban railway noise.

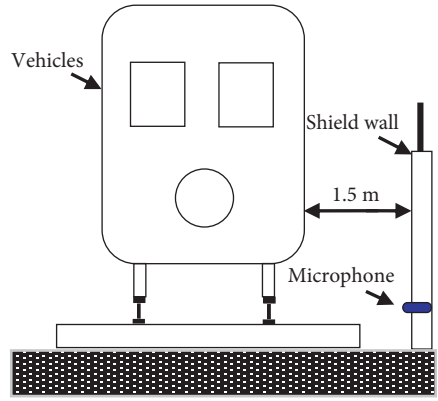

Figure 1: Measurement scheme diagram.

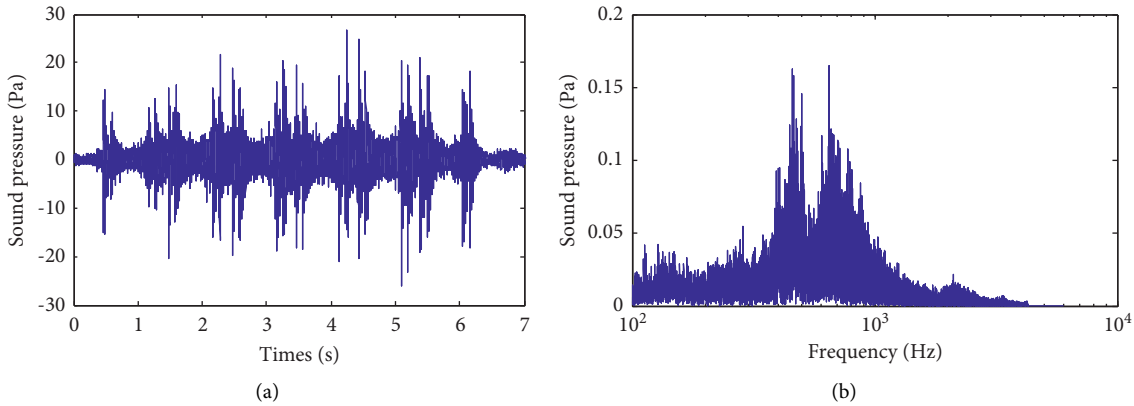

Figure 2: Sound pressure of urban railway: (a) time domain and (b) frequency domain.

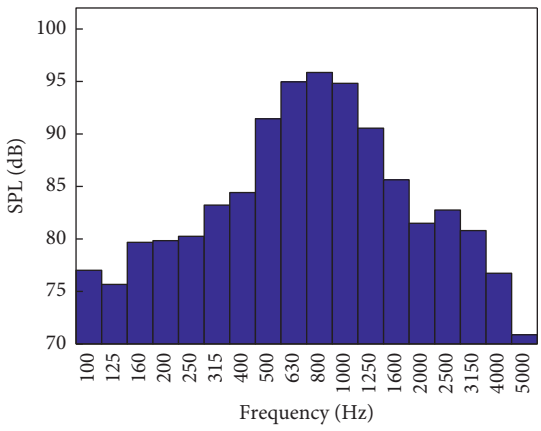

Figure 3: 1/3 octave spectrum.

3. Designing and Modeling

3.1. Designing. The acoustic energy harvester is composed of a Helmholtz resonator and a piezoelectric circular plate. The structure is shown in Figure 4(a). The Helmholtz resonator is composed of a neck and a cavity. The sound pressure is amplified by the Helmholtz resonator and then acts on the piezoelectric circular plate. The dynamic bending of the piezoelectric circular plate creates tensile and compressive strains in the piezoelectric layers, which generate charges on the electrodes via piezoelectric effect. The electrodes are connected to a load resistance standing for an electric load. The cutaway view of the harvester is shown in Figure 4(b). The radius and the length of the neck are $r_n = 10$ mm and $L_n = 10$ mm, respectively. The radius and the length of the cavity are $r_c = 25$ mm and $L_c = 27$ mm, respectively.

A thin circular piezoelectric plate is made of a brass plate and a piezoelectric plate. The structure is shown in Figure 4(b). The radius and the thickness of the brass plate are $R = 25$ mm and $h_b = 0.2$ mm, respectively. The thickness of the piezoelectric plate is $h_p = 0.2$ mm. In addition, the rim of the circular plate is clamped by the bottom of the Helmholtz resonator. The PZT-5H piezoelectric ceramic is used in the harvester. The surface of the piezoelectric plate consists of silver electrodes.

3.2. Model of Helmholtz Resonator. The Helmholtz resonator is simplified into a mass spring system [4], as shown in Figure 5(b).

Based on Newton's second law of motion, the equation for the mass spring system is

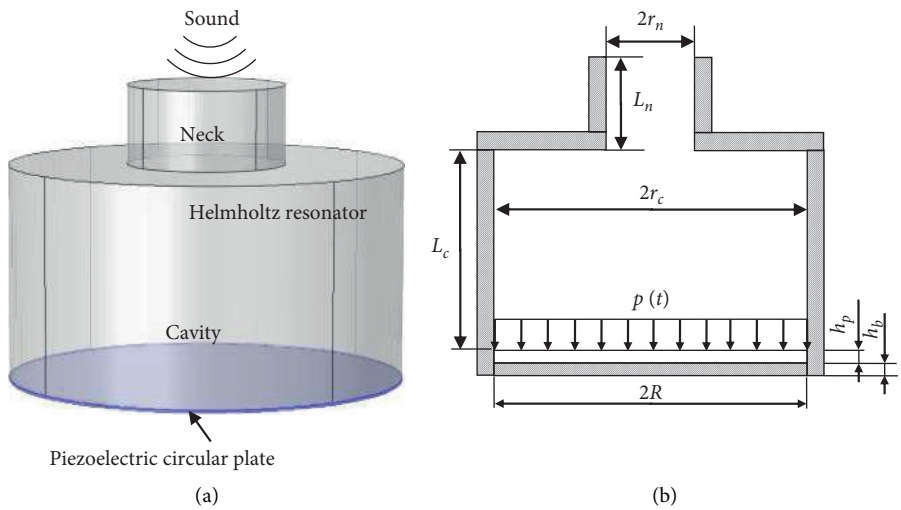

Figure 4: Design of acoustic energy harvester: (a) axonometric drawing and (b) cutaway view.

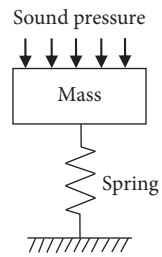

Figure 5: Spring-mass model of Helmholtz resonator.

$$m\frac{\mathrm{d}^2x}{\mathrm{d}t^2} = (P_n - P_c)A_n, \tag{1}$$

where $m = \rho A_n L_{\text{eff}}$ is the mass of the air in the neck, ρ is the density of air, and A_n is the cross-sectional area of the neck. $L_{\text{eff}} = L_n + 1.7r_n$ is the effective length of neck. Moreover, P_n is the incident sound pressure amplitude, and P_c is the sound pressure amplitude in bottom of the cavity.

According to the equation of state for ideal gas (Ruan et al., 2006), the equation of the gas in the Helmholtz resonator can be written as

$$\mathrm{P}v^{\gamma} = \text{const}, \tag{2}$$

where $v = 1/\rho$ is the volume of the gas and γ is the adiabatic index.

By determining the differential to equation (2), we can obtain

$$\mathrm{d}P = -P\gamma\frac{\mathrm{d}v}{v} = -P\gamma\frac{\mathrm{d}V_c}{V_c}. \tag{3}$$

In an adiabatic ideal gas, the velocity of sound can be expressed as $c = \sqrt{\gamma P/\rho}$. Thus, equation (3) can be expressed as

$$\mathrm{d}P = \rho c^2\frac{\mathrm{d}v}{v}. \tag{4}$$

During a very short time, the change of P_n and P_c is small. Thus, we believe that $\rho\,\rho_0$, $c \approx c_0$, and $P_c \approx \mathrm{d}P$.

$$P_c = -\rho_0 c_0^2\frac{\mathrm{d}V_c}{V_c}. \tag{5}$$

Substituting $dV_c = -A_n x$ with equation (5), we have

$$P_c = \frac{\rho_0 c_0^2 A_n}{V_c}x. \tag{6}$$

Substituting equation (6) with equation (1), we can obtain

$$m\frac{\mathrm{d}^2x}{\mathrm{d}t^2} + kx = P_n A_n, \tag{7}$$

where the elasticity coefficient of the equivalent spring is $k = \rho_0 c_0^2 A_n^2/V_c$. The solution of equation (7) is

$$x = \frac{P_n A_n}{k - \omega^2 m}. \tag{8}$$

When resonance occurs, we can obtain $k - \omega^2 m = 0$. Thus, we have

$$\frac{\rho_0 c_0^2 A_n^2}{V_c} - \rho_0 L_{\text{eff}} A_n \omega^2 = 0. \tag{9}$$

The resonant frequency of the Helmholtz resonator can be written as

$$f_r = \frac{c_0}{2\pi}\sqrt{\frac{A_n}{V_c L_{\text{eff}}}}, \tag{10}$$

where c_0 is the speed of sound in air. The sound pressure amplification factor of the Helmholtz resonator is expressed as

$$G = \frac{P_c}{P_n} = \frac{c_0^3}{(2\pi)^2 f_r^3 V_c} = 2\pi\sqrt{V_c\left(\frac{L_{\text{eff}}}{A_n}\right)^3}. \tag{11}$$

From equations (10) and (11), the resonant frequency increased with the increase of the cross-sectional area of the neck. Then it decreased with the increase of the effective length of the neck and the volume of the cavity. The sound pressure amplification factor of the Helmholtz resonator increased with the increase of the cross-sectional area of the neck, the effective length of the neck, and the volume of the cavity.

3.3. Model of Piezoelectric Circular Plate. The dynamic sound pressure $p(t)$ is provided by the Helmholtz resonator. The dynamic bending of the plate creates tensile and compressive strains in the piezoelectric layers, which generate charges on the electrodes via piezoelectric effect. The electrodes are connected to a load resistance standing for an electric load.

The bending differential equation of the piezoelectric circular plate is

$$\frac{d}{\mathrm{d}r}\left[\frac{1}{r}\frac{d}{\mathrm{d}r}\left(r\frac{\mathrm{d}w}{\mathrm{d}r}\right)\right] = \frac{Q_r}{D}, \tag{12}$$

where w is the deflection and D is the equivalent flexural rigidity of piezoelectric circular plate. Substituting the shear stress $Q_r = \pi r^2 p/2\pi r = pr/2$ with equation (12), we can obtain

$$\frac{d}{\mathrm{d}r}\left[\frac{1}{r}\frac{d}{\mathrm{d}r}\left(r\frac{\mathrm{d}w}{\mathrm{d}r}\right)\right] = \frac{pr}{2D}. \tag{13}$$

Solving equation (13), we can obtain

$$w = \frac{pr^4}{64D} + \frac{C_1 r^2}{4} + C_2 \ln r + C_3, \tag{14}$$

where C_1, C_2, and C_3 are integral constants. In the center of the piezoelectric circular plate, the angle of deflection surface and the deflection is a limited value. Thus, $C_2 = 0$. C_1 and C_3 are determined by boundary conditions.

The boundary conditions can be expressed as equation (15) due to the sides of the piezoelectric circular plate with simple supported constraints.

$$\begin{cases} r = R, & w = 0, \\ r = R, & M_r = 0. \end{cases} \tag{15}$$

Substituting equation (15) with equation (14), we can obtain

$$w = \frac{p(t)}{64D}\left[\left(R^2 - r^2\right)^2 + \frac{4R^2\left(R^2 - r^2\right)}{1+\lambda}\right], \tag{16}$$

where λ is the equivalent Poisson's ratio of the piezoelectric circular plate. The curvature differential equation of the piezoelectric circular plate can be expressed as

$$K = \frac{1}{\rho(x)} = \frac{\left|w''(r,t)\right|}{\left[1 + w'^2(r,t)\right]^{3/2}} \approx \left|w''(r,t)\right| = \frac{p(t)}{16D}\left|3r^2 - \frac{R^2(3+\lambda)}{1+\lambda}\right|. \tag{17}$$

The position of the neutral layer of the piezoelectric circular plate is

$$h = \frac{RE_bT_b^2 + RE_pT_p^2 + 2RE_pT_pT_b}{2RE_pT_p + 2RE_bT_b}. \tag{18}$$

The distribution of the axial strain of the piezoelectric circular plate in the thickness direction is linear [33]. The axial strain distribution function of the piezoelectric circular plate is

$$S(r,t) = T_m K(r,t) = \begin{cases} \dfrac{p(t)T_m}{16D}\left(\dfrac{R^2(3+\lambda)}{1+\lambda} - 3r^2\right) & r \in \left[0, \dfrac{R\sqrt{3+\lambda}}{\sqrt{3(1+\lambda)}}\right), \\ \dfrac{p(t)T_m}{16D}\left(3r^2 - \dfrac{R^2(3+\lambda)}{1+\lambda}\right) & r \in \left[\dfrac{R\sqrt{3+\lambda}}{\sqrt{3(1+\lambda)}}, R\right], \end{cases} \tag{19}$$

where $T_m = 0.5h_p + h_b - h$ is the axial distance from each point of the piezoelectric circular plate to the neutral layer.

The electric charge $Q(t)$ on the electrode surface can be calculated by using the first kind of piezoelectric equation.

$$Q(t) = \frac{\pi d_{31} p(t) T_m R^4 \left(5\lambda^2 + 6\lambda + 9\right)}{96 s_{11}^E D (1+\lambda)^2} + \pi R^2 \bar{\varepsilon}_{33} E_3(t), \tag{20}$$

where d_{31} is the piezoelectric constant, E_3 is the electric field, $\bar{\varepsilon}_{33}$ is the one-dimensional dielectric permittivity, and s_{11}^E is the elastic compliance constant.

Output current $i(t)$ can be expressed as

$$i(t) = \frac{\pi d_{31} T_m R^4 \left(5\lambda^2 + 6\lambda + 9\right)}{96 s_{11}^E D (1+\lambda)^2} \frac{\mathrm{d}p(t)}{\mathrm{d}t} - \frac{\pi R^2 \bar{\varepsilon}_{33}}{T_p} \frac{\mathrm{d}u(t)}{\mathrm{d}t}. \tag{21}$$

The sound pressure can be expressed as $p(t) = p\sin(\omega t)$. Based on the equation $u(t) = i(t) R_L$, the output voltage is

$$u(t) = \frac{\pi d_{31} T_p T_m R^4 \left(5\lambda^2 + 6\lambda + 9\right) \omega p_i R_L}{96 s_{11}^E D (1+\lambda)^2 \sqrt{T_p^2 + \omega^2 R_L^2 \left(\pi R^2 \bar{\varepsilon}_{33}\right)^2}} \sin(\omega t), \tag{22}$$

where R_L is the load resistance. The output power can be expressed as

$$P(t) = \frac{u(t)^2}{R_L}. \tag{23}$$

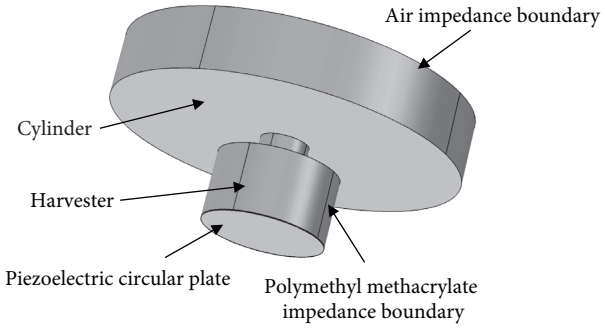

Figure 6: Geometry of finite element model of harvester.

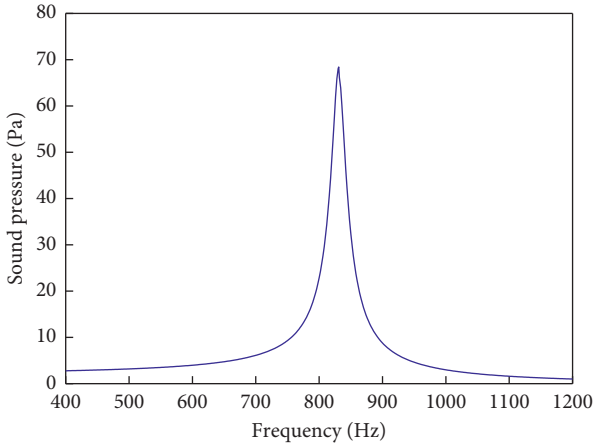

Figure 7: Frequency response of Helmholtz resonator.

4. Simulation Results

4.1. Simulations of Helmholtz Resonator. The finite element analysis model of the Helmholtz resonator is established in the COMSOL Multiphysics®. The material of the Helmholtz resonator is polymethyl methacrylate. A cylinder is added at the top of the Helmholtz resonator. This cylinder represents the volume of air that enters the Helmholtz resonator. The boundary of the Helmholtz resonator is polymethyl methacrylate impedance boundary, and the boundary of the cylinder is the air impedance boundary. The plane wave acts on the surface of the cylinder as the excitation. The finite element analysis model is shown in Figure 6. In simulation, the density, elastic modulus, and Poisson's ratio of the polymethyl methacrylate are 1160 kg/m^3, 2.8 GPa, and 0.36, respectively. The damping factor of the brass plate is 0.002 and the dielectric loss of the piezoelectric film is 0.02. The dynamic viscosity coefficient of the air is 15.11×10^{-6} m^2/s.

Figure 7 shows the frequency response of the Helmholtz resonator. The incident sound pressure is 2 Pa. As can be seen from the figure, sound pressure also increases rapidly within the frequency band of 700–900 Hz. The resonant frequency of the Helmholtz resonator is 831 Hz.

Figures 8(a) and 8(b) show the sound pressure response and the sound pressure isosurface of the circular plate acoustic energy harvester, respectively, when the circular plate acoustic energy harvester is resonant. The sound pressure reaches its maximum value of 68.473 Pa when it approaches the end of the Helmholtz resonator. In addition, the sound pressure amplification factor is 34.24.

4.2. Simulations of Circular Piezoelectric Plate. The finite element analysis model of the circular piezoelectric plate is also established. The model is shown in Figure 9. The circular piezoelectric plate is made up of two parts: the brass substrate and the PZT-5H piezoelectric film. The parameters are listed in Table 1.

Figure 10 shows the first-order vibration modal result and frequency of the circular piezoelectric plate. The first-order natural frequency of the circular piezoelectric plate is 831.7 Hz. According to the theoretical model in Section 3.3, the theoretical natural frequency is 812 Hz, and the error is 2.98%. Figure 11 shows the deformation of the circular piezoelectric plate with the Helmholtz resonator. The frequency of the excitation sound is 831 Hz. The simulation result of the deformation is 1.4623×10^{-3}. In addition, the theoretical result of the deformation is 1.3284×10^{-3} according to Section 3.3. The error is 10.08%. These results demonstrate the accuracy of the theoretical model.

The radius of piezoelectric plate has a great influence on the resonance frequency, so it is set as a constant in the simulation. In addition, the radius of piezoelectric plate is related to its capacitance C_p. The larger the radius of the

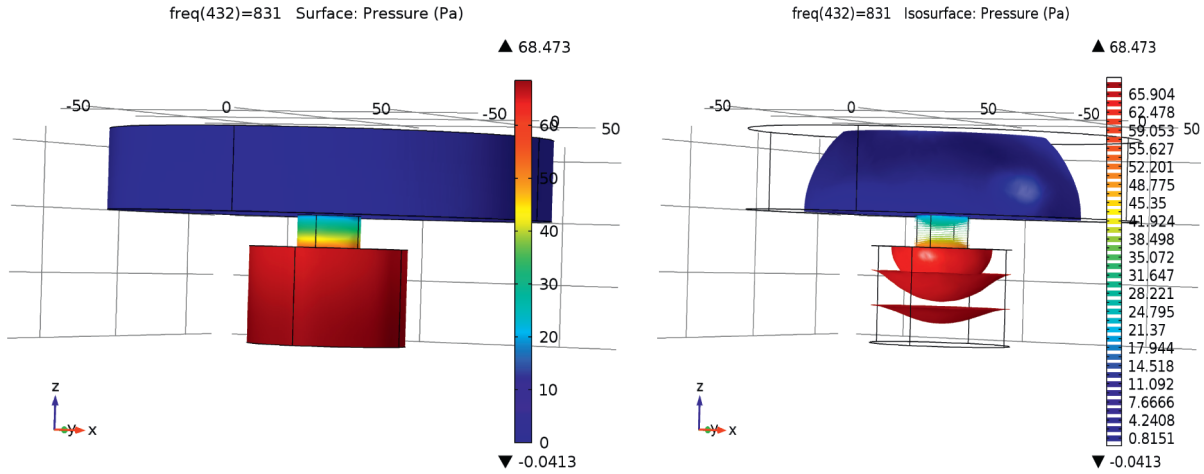

(a) (b)

Figure 8: Simulation results of Helmholtz resonator: (a) sound pressure response and (b) sound pressure isosurface.

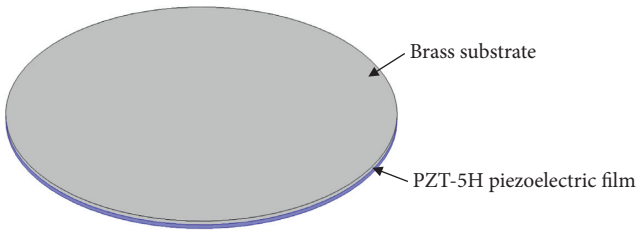

Figure 9: Finite element model of circular piezoelectric plate.

Table 1: Parameters of the PZT-5H piezoelectric film.

Parameters	Unit	PZT-5H	Brass
Density	kg/m^3	7600	8920
Elastic modulus	GPa	60.6	106
Poisson's ratio	/	0.34	0.35
Piezoelectric constant	m/V	$274e^{-12}$	/
Dielectric constant	F/m	$3.363e^{-8}$	/
Elastic compliances constant	m^2/N	$16.5e^{-12}$	/

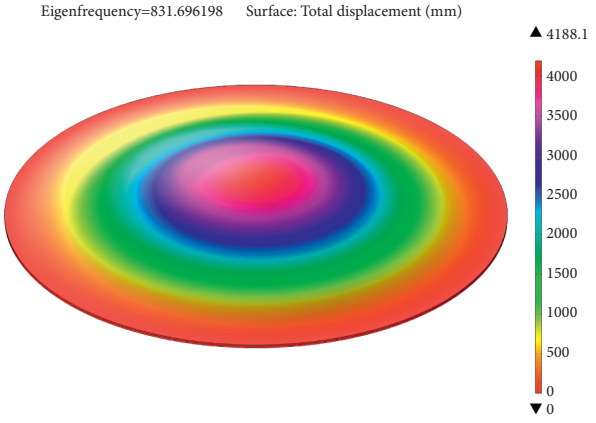

Figure 10: Modal analysis result of piezoelectric circular plate.

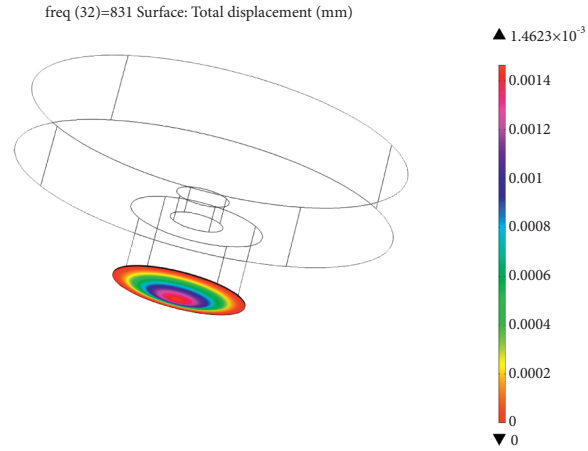

Figure 11: Displacement of piezoelectric circular plate with Helmholtz resonator.

piezoelectric plate, the larger the capacitance value. The load resistance R_L, capacitance C_p, and the vibration frequency f meet the following relationship: $R_L = 1/2\pi f C_p$. So the radius of the piezoelectric plate should be large enough to reduce the load resistance. In the simulation, the radius of piezoelectric plate is the same as the brass substrate.

4.3. Simulations of Harvester under Urban Railway Noise. The traffic line of Shanghai Metro is totally closed. For safety reasons, the authors are not allowed to enter the line and test the performance of the harvester under the real excitation of the urban railway noise. So the authors use the data of the urban railway noise and study the harvester by simulation.

Figure 12 shows the time domain of the sound pressure with the Helmholtz resonator. The excitation sound is the urban railway noise in Section 2. The maximum sound pressure can reach 80 Pa, and the main frequency is 800 Hz.

By using the Runge–Kutta method, the theoretical model of the harvester is solved. Figure 13(a) shows the curves of

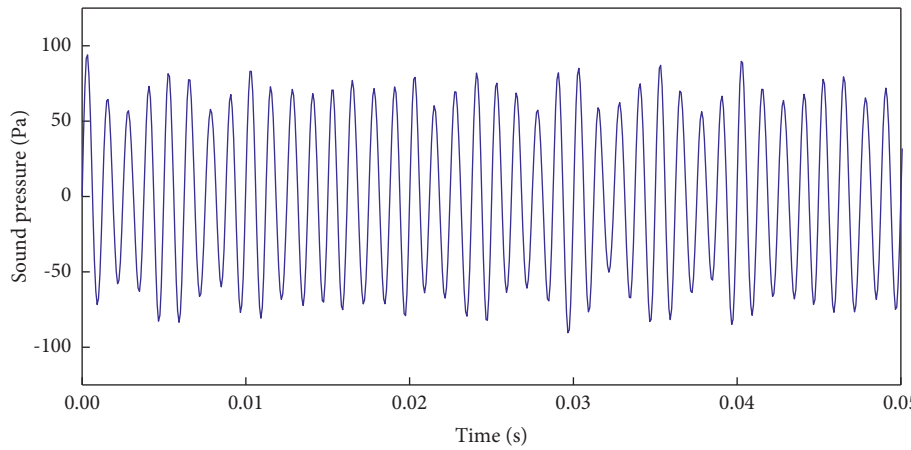

Figure 12: Sound pressure with Helmholtz resonator.

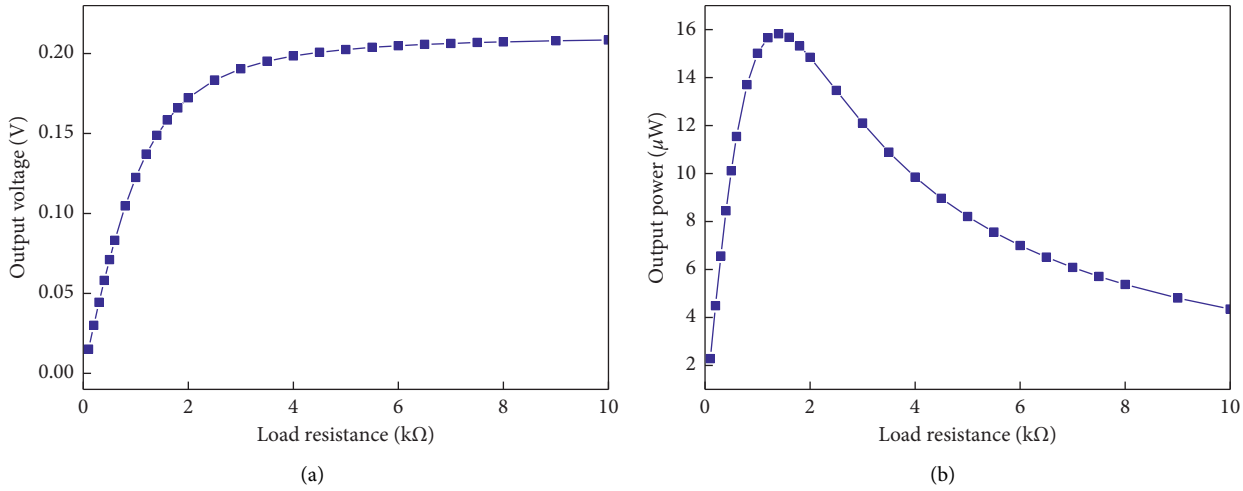

Figure 13: Voltage and power response with different resistance: (a) resistance-voltage curve and (b) resistance-power curve.

the resistance-voltage relationship. The maximum voltage increases with the resistance and tends to a constant for the resistance beyond 6 kΩ. Figure 13(b) shows the curves of the resistance-power relationship. The maximum power is not monotonous with the change of the resistance, and it reaches its peak value when the load resistance R_L approaches 1.4 kΩ.

The load resistance R_L is set as 1.4 kΩ. Figure 14 shows the output voltage of the harvester. The max output voltage is 0.149 V. Figure 15 shows the output power of the harvester. The peak value of the output power is approximately 25 μW and the RMS value of the output power is 15.825 μW. These simulation results demonstrate that the circular plate energy harvester with the Helmholtz resonator can effectively harvest the urban railway noise.

5. Experimental Validations

5.1. Experiment Device. The experiment system is presented in Figure 16 and the photos are shown in Figure 17. The speaker is used to generate an incident sound wave. The signal used to drive the speaker is generated by the DQA module (AVAVT-MI7016) and amplified by the power amplifier. Microphone 1 (AWA14425) is used to measure the incident sound pressure, and microphone 2 (AWA14425) is used to measure the sound pressure in the cavity. The signals are also recorded by the DQA module (AVAVT-MI7016). The output voltage is measured by the oscilloscope (HIOKI 8860–50). In addition, the plane wave tube is an important device in the experiment system. The wall of the plane wave tube should be rigid and smooth, so it is made aluminum and have sufficient thickness and weight. In order to avoid vibration caused by sound waves, the length of the tube (l), the diameter of tube (d), the lower limit of acoustic frequency (f), and the sound velocity (c) should meet the following relationship: $l \geq 0.75/f + 3d$.

In the experiment system, the Helmholtz resonator is made of polymethyl methacrylate. The thin plate at the bottom of the Helmholtz resonator was assembled by the brass plate and the piezoelectric plate (PZT-5H). The harvester was installed at the bottom of the plane wave tube. A small hole (the diameter is less than 5 mm) was drilled through the Helmholtz resonator to install microphone 2.

5.2. Results of Experiment. Figure 18 shows the amplitude-frequency responses of the Helmholtz resonator. The red-dashed line represents the theoretical results based on equations

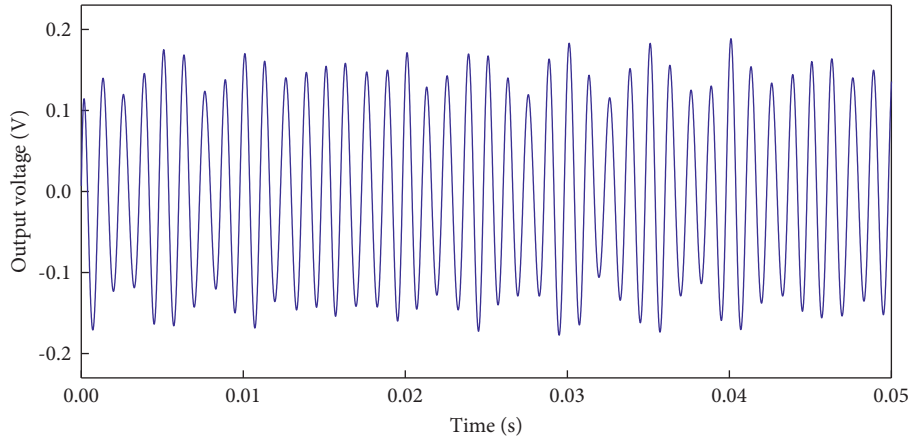

Figure 14: Output voltage of harvester under urban railway noise.

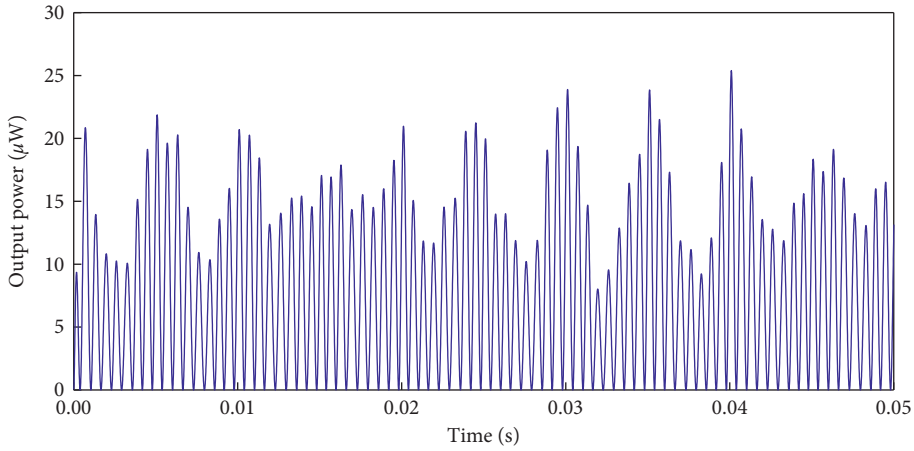

Figure 15: Output power of harvester under urban railway noise.

(10) and (11). The blue solid line denotes the results of the experiment, and the dash-dotted line is the incident sound pressure. The incident sound pressure is 2 Pa (100 dB). The resonance frequency of the circular plate acoustic energy harvester is approximately 836 Hz, and the sound pressure amplification factor is 34.31. The theoretical results are compared with the results of the experiment and show good agreement.

Figure 19 shows the open circuit output voltage of the proposed harvester. As shown in the figure, the blue solid line represents the simulation results, and the red line with the scatters signifies the results of the experiment. Although the voltage of the experiment is higher than that of the simulation results, the trend of the results of the experiment and the simulation results are consistent. The peak value is at 830 Hz, which is the resonance frequency of the harvester.

Figure 20 shows that the output voltage and the power are shown with the variable load resistance from 5 Ω to 5 kΩ. The incident sound is 2 Pa (100 dB) at 830 Hz. The output voltage increases with the increasing load resistance and tends to a certain constant after the load resistance is larger than 3 kΩ. The power achieves its maximum when the resistance is 0.8 kΩ. The peak output power is 8.452 μW, and the corresponding voltage is 0.082 V. The simulation results and the measured results show good agreement. It demonstrates that the proposed models in Section 3 can describe the developed acoustic energy harvester of urban railways. The optimal output power is 8.452 μW, which is higher than the output power at 1.24 μW in [23]. The volume of the developed harvester is 56.16 cm^3, and the output power density is 0.15 $\mu W/cm^3$. The volume of the harvester in [23] is about 112.51 cm^3, and the output power density is 0.011 $\mu W/cm^3$. Therefore, the proposed harvester in the study performs better than that in literature.

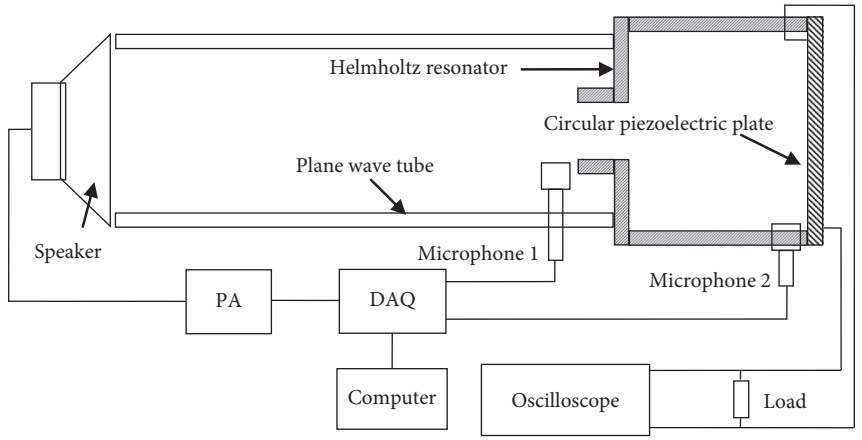

Figure 16: Experiment setup.

(a) (b)

Figure 17: The photos of the experiment system: (a) experiment setup and (b) acoustic energy harvester.

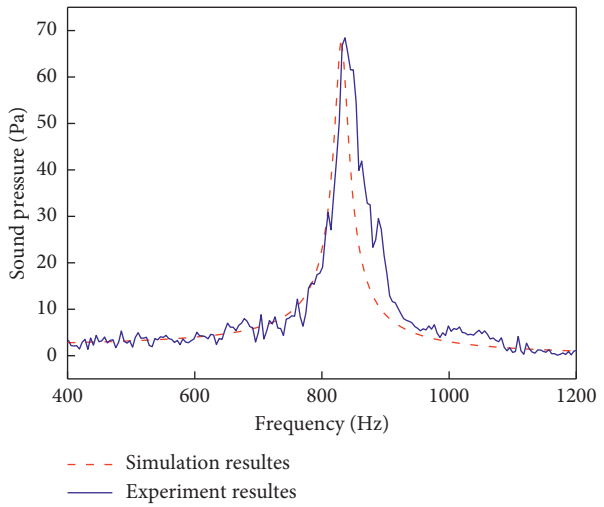

Figure 18: Comparisons of experiment results and simulation results of Helmholtz resonator.

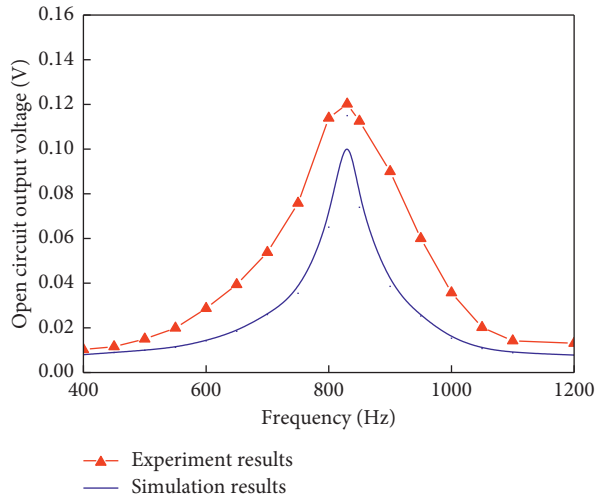

Figure 19: Frequency response of open circuit output voltage.

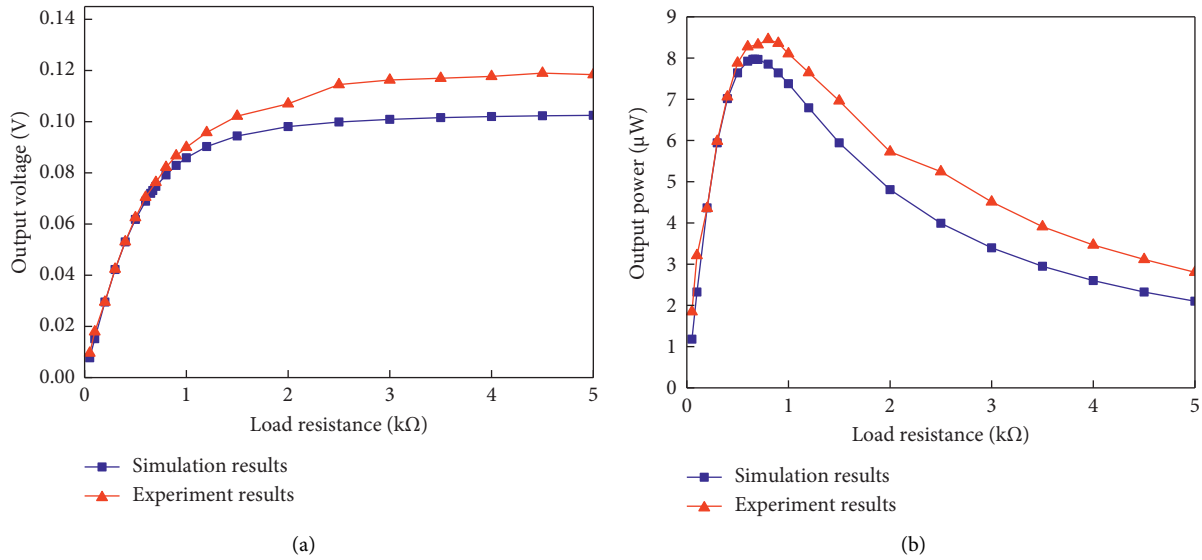

Figure 20: Voltage and power response with different resistance: (a) resistance-voltage curves and (b) resistance-power curves.

6. Conclusions

This investigation developed a novel circular plate energy harvester for urban railway noise. The harvester consists of a Helmholtz resonator and a circular piezoelectric plate. The circular plate energy harvester with the Helmholtz resonator is analytically, numerically, and experimentally investigated. The simulation results and the experiment results show good agreement. Moreover, the results demonstrate that the harvester with the Helmholtz resonator can effectively harvest the urban railway noise. The investigation yields the following conclusions:

(1) The urban railway noise includes various frequencies. The noise energy is mainly concentrated within the frequency band of 400–1600 Hz, and the maximum noise energy appears in the 800 Hz frequency band.

(2) The resonant frequency and amplification ratio of the developed Helmholtz resonator are 836 Hz and 34.31, respectively. The results of the experiment are in good agreement with the simulation results.

(3) Through simulation investigation, the maximum output power of the harvester is approximately 25 μW and the maximum voltage is 0.149 V under the excitation of the urban railway noise. The simulation results demonstrate that the harvester with the Helmholtz resonator can effectively harvest the urban railway noise.

(4) Under the excitation of 2 Pa (830 Hz) in the experiment, the maximum output power of the circular plate acoustic energy harvester is approximately 8.452 μW, and the maximum voltage is 0.082 V.

Data Availability

The data used to support the findings of this study are available from the corresponding author upon request.

Conflicts of Interest

The authors declare that they have no conflicts of interest.

Acknowledgments

This work was supported by the National Natural Science Foundation of China (nos. 11802170, 51575334, and U1834201), 2018 Shanghai "Chenguang Project" (no. 18CG66), and Natural Science Foundation of Shanghai (no. 19ZR1421700).

References

[1] D. W. Wang, M. X. Liu, W. J. Qian, X. Wu, and Z. Q. Wu, "Parametrical investigation of piezoelectric energy harvesting via friction-induced vibration," *Shock and Vibration*, vol. 2020, Article ID 6190215, 32 pages, 2020.

[2] S. Duan, W. Q. Song, E. Zio, C. Cattani, and M. Li, "Product technical life prediction based on multi-modes and fractional Lévy stable motion," *Mechanical Systems and Signal Processing*, vol. 161, no. 12, Article ID 107974, 2021.

[3] A. X. Luo, Y. L. Zhang, X. T. Dai et al., "An inertial rotary energy harvester for vibrations at ultra-low frequency with high energy conversion efficiency," *Applied Energy*, vol. 279, Article ID 115762, 2020.

[4] M. A. Pillai and E. Deenadayalan, "A review of acoustic energy harvesting," *International Journal of Precision Engineering and Manufacturing*, vol. 15, no. 5, pp. 949–965, 2014.

[5] R. Ahmed, F. Mir, and S. Banerjee, "A review on energy harvesting approaches for renewable energies from ambient vibrations and acoustic waves using piezoelectricity," *Smart Materials and Structures*, vol. 26, no. 8, Article ID 085031, 2017.

[6] H. Lin, M. He, Q. Jing et al., "Angle-shaped triboelectric nanogenerator for harvesting environmental wind energy," *Nanomaterials and Energy*, vol. 56, pp. 269–276, 2019.

[7] M. Bagmanci, M. Karaaslan, E. Unal, O. Akgol, M. Bakır, and C. Sabah, "Solar energy harvesting with ultra-broad band metamaterial absorber," *International Journal of Modern Physics B*, vol. 33, no. 8, Article ID 1950056, 2019.

[8] L. Xu, T. Jiang, P. Lin et al., "Coupled triboelectric nanogenerator networks for efficient water wave energy harvesting," *ACS Nano*, vol. 12, no. 2, pp. 1849–1858, 2018.

[9] Z. Q. Lu, D. H. Gu, D. Hu, W. Lacarbonara, and L. Q. Chen, "Nonlinear vibration isolation via a circular ring," *Mechanical Systems and Signal Processing*, vol. 136, Article ID 106490, 2020.

[10] V. Pakrashi, G. Marano, P. Cahill, S. F. Ali, and M. Magno, "Vibration energy harvesting for monitoring dynamical systems," *Shock and Vibration*, vol. 2018, Article ID 8396029, 2 pages, 2018.

[11] Y. L. Zhang, A. X. Luo, Y. F. Wang, X. T. Dai, Y. Lu, and F. Wang, "Rotational electromagnetic energy harvester for human motion application at low frequency," *Applied Physics Letters*, vol. 116, no. 5, Article ID 053902, 2020.

[12] M. A. Halim, K. Tao, S. Towfighian, and D. Zhu, "Vibration energy harvesting: linear, nonlinear, and rotational approaches," *Shock and Vibration*, vol. 2019, Article ID 5381756, 2 pages, 2019.

[13] X. G. Guo, Y. L. Zhang, K. Q. Fan, C. K. Lee, and F. Wang, "A comprehensive study of non-linear air damping and "pull-in" effects on the electrostatic energy harvesters," *Energy Conversion and Management*, vol. 203, Article ID 112264, 2020.

[14] C. Y. Zhang, G. Hu, Y. Daniil et al., "Machine learning based prediction of piezoelectric energy harvesting from wake galloping," *Mechanical Systems and Signal Processing*, vol. 160, Article ID 107876, 2021.

[15] Y. Peng, D. Zhang, J. Luo, S. R. Xie, H. Y. Pu, and Z. J. Li, "Power density improvement based on investigation of initial relative position in an electromagnetic energy harvester with self-powered applications," *Smart Materials and Structures*, vol. 30, no. 6, Article ID 065005, 2021.

[16] X. Lei, "Methods for predicting the ambient vibration and noise resulting from rail transit," *Proceedings of the Institution of Mechanical Engineers - Part F: Journal of Rail and Rapid Transit*, vol. 234, no. 9, pp. 1054–1067, 2020.

[17] B. Li, J. H. You, and Y. J. Kim, "Low frequency acoustic energy harvesting using PZT piezoelectric plates in a straight tube resonator," *Smart Materials and Structures*, vol. 22, no. 5, Article ID 055013, 2013.

[18] W. T. Gao, J. P. Xia, H. X. Sun, S. Q. Yuan, G. Yong, and X. J. Liu, "Acoustic energy harvesting for low-frequency airborne sound based on compound mie resonances," *Applied Physics Express*, vol. 12, no. 4, Article ID 044002, 2019.

[19] M. Yuan, Z. P. Cao, J. Luo, and R. Ohayon, "Acoustic metastructure for effective low-frequency acoustic energy harvesting," *Journal of Low Frequency Noise, Vibration and Active Control*, vol. 37, Article ID 146134841879483, 2018.

[20] H. Y. Lee and B. Choi, "A multilayer PVDF composite cantilever in the Helmholtz resonator for energy harvesting from sound pressure," *Smart Materials and Structures*, vol. 22, no. 11, p. 5025, 2013.

[21] S. Noh, H. Lee, and B. Choi, "A study on the acoustic energy harvesting with Helmholtz resonator and piezoelectric cantilevers," *International Journal of Precision Engineering and Manufacturing*, vol. 14, no. 9, pp. 1629–1635, 2013.

[22] A. C. Yang, P. Li, and Y. M. Wen, "High-efficiency broadband acoustic energy harvesting using Helmholtz resonator and

dual piezoelectric cantilever beams," *Review of Scientific Instruments*, vol. 85, no. 6, pp. 15–35, 2014.

[23] Y. Wang, X. Zhu, T. Zhang et al., "A renewable low-frequency acoustic energy harvesting noise barrier for high-speed railways using a Helmholtz resonator and a PVDF film," *Applied Energy*, vol. 230, pp. 52–61, 2018.

[24] H. M. Noh, "Acoustic energy harvesting using piezoelectric generator for railway environmental noise," *Advances in Mechanical Engineering*, vol. 10, no. 7, Article ID 168781401878505, 2018.

[25] M. Yuan, Z. Cao, J. Luo, and Z. Pang, "Helix structure for low frequency acoustic energy harvesting," *Review of Scientific Instruments*, vol. 89, Article ID 055002, 2018.

[26] A. B. Atrah and H. Salleh, "Simulation of acoustic energy harvester using Helmholtz resonator with piezoelectric backplate," in *Proceedings of the 20th International Congress on Sound & Vibration*, ICSV20, Bangkok, Thailand, July 2013.

[27] F. Khan Izhar, "Piezoelectric type acoustic energy harvester with a tapered Helmholtz cavity for improved performance," *Journal of Renewable and Sustainable Energy*, vol. 8, no. 5, pp. 705–709, 2016.

[28] T.-C. Yuan, J. Yang, and L.-Q. Chen, "Nonlinear vibration analysis of a circular composite plate harvester via harmonic balance," *Acta Mechanica Sinica*, vol. 35, no. 4, pp. 912–925, 2019.

[29] X. Zhao, T. Q. Yang, Y. Dong, and X. C. Wang, "Energy harvester array using piezoelectric circular diaphragm for broadband vibration," *Applied Physics Letters*, vol. 104, no. 22, Article ID 223904, 2014.

[30] J. Yuan, T. Xie, W. Chen, X. Shan, and S. Jiang, "Performance of a drum transducer for scavenging vibration energy," *Journal of Intelligent Material Systems and Structures*, vol. 20, no. 14, pp. 1771–1777, 2009.

[31] T.-C. Yuan, J. Yang, and L.-Q. Chen, "Nonlinear dynamics of a circular piezoelectric plate for vibratory energy harvesting," *Communications in Nonlinear Science and Numerical Simulation*, vol. 59, pp. 651–656, 2018.

[32] H. Hongping Hu and H. P. Hu, "Nonlinear characteristics of a circular plate piezoelectric harvester with relatively large deflection near resonance," *IEEE Transactions on Ultrasonics, Ferroelectrics, and Frequency Control*, vol. 55, no. 9, pp. 2092–2096, 2008.

[33] T. C. Yuan, J. Yang, and X. W. Liu, "Vibration energy harvesting system for railroad safety based on running vehicles," *Smart Materials and Structures*, vol. 23, Article ID 125046, 2014.